J Integr Sci Technol, 2014, 2(1), 13-21 Article

Journal of Integrated
Science and Technology

Structural analysis and dielectric characterization of Aurivillius type $CaSrBi_2Nb_2O_9$ ceramics

S. Khasa,[a] Paramjeet Singh,[b] Sujata Sanghi,[b] Navneet Singh,[b] and Ashish Agarwal[b*]

[a]Department of Physics, Deenbandhu Chhoturam University of Science & Technology, Murthal, Sonepat, Haryana, India-131039
[b]Department of Physics, Guru Jambheshwara University of Science & Technology, Hisar, Haryana, India-125001

Received 25 July, 13

ABSTRACT

This work describes synthesis of powdered materials belonging to the Aurivillius oxide family (Bi2O2)2+(An-1BnO3n+1)2- for n = 2 and provides an approach for understanding the structural evolution with composition. The effect of strontium doping on the lattice response and dielectric properties of Ca1-xSrxBi2Nb2O9 (x = 0.0, 0.5, 1.0) ferroelectric ceramics is studied. The XRD studies revealed single phase formation of orthorhombic structure. The average crystallite size was obtained in the range 22-41 nm. The dielectric properties, viz. dielectric constant, loss tangent and ac electrical conductivity of the samples were studied by using impedance spectroscopy. A strong low frequency dielectric dispersion was found to exist in these samples. Its occurrence was ascribed to the presence of ionized space charge carriers such as oxygen vacancies. The relationship among doping, crystal structure, and dielectric properties were also discussed. Measurements of the dielectric permittivity as a function of temperature reveal signs of single phase transition. The thermal activation energy for the grain electric conductivity was lower in the high temperature region (Ea(ht) = 0.08 eV) and higher in the low temperature region (Ea(lt) = 0.21 eV).

Keywords: Aurivillius oxide, impedance spectroscopy, electrical conductivity, solid-state reaction.

Introduction

In 1950s, Aurivillius synthesized a new series of layered ceramics, which contained Bismuth layer as a structural constraint. The role of bismuth layer in influencing the electrical and ferroelectric properties of these ceramics has been found to be crucial.[1-6] Recently, capacitors based on layered perovskites such as $CaBi_2Nb_2O_9$ (CBNO) and metallic electrodes, such as Pt, have generated interest because of their negligible polarization fatigue (> 10^{12} cycles), long polarization retention, and very low leakage current.[7-12]But the major limitations for the application of CBNO are the high processing temperature (~800-1000°C) and low remnant polarization compared to the processing temperature of 600°C for PZT ceramics.[13]

Address:
Ashish Agarwal
Department of Physics,Guru Jambheshwara University of Science & Technology, Hisar, Haryana, India-125001
Tel: +919416672988
Email: aagju@yahoo.com

Cite as: *J. Integr. Sci. Technol, 2014, 2(1), 13-21*

The high processing temperature of CBNO makes it not easy to match the process of very-large-size-integrated circuits (VLSI) fabrication to produce high quality non-volatile memory. One of the approaches to solve the problem is to lower the CBNO processing temperature and the other is to solve the problems caused by the high processing temperature. It has been found that the thin film of CBNO demonstrates their excellent fatigue endurance and has a significant influence on the ferroelectric properties.[14, 15] The grain size of the polycrystal CBNO thin film plays an important role in improving the CBNO capacitor ferroelectric properties. It has been noticed that minimum ferroelectric properties are exhibited only when the grain approach a critical size.[15] Therefore it may be a good way to achieve a higher remnant polarization and lower processing temperature by forming solid solutions of CBNO with another ferroelectric material, which has higher remnant polarization, larger grain size and lower processing temperature. Some CBNO-based solid solutions, especially CBNO/SBTO have been studied in the past[16] but the dielectric properties of these ceramics are yet to be investigated experimentally.

In the present study we have prepared solid solutions of $Ca_{1-x}Sr_xBi_2Nb_2O_9$ ceramics (with x = 0.0, 0.5, 1.0). These kind of ceramics belong to a family of oxides with a general formula $(Bi_2O_2)^{2+}(A_{n-1}B_nO_{3n+1})^{2-}$ where, n = 1,2,3,4,5 representing the number of layers. The structure consists of $(Bi_2O_2)^{2+}$ layers, made up of oxygen octahedral, interleaved with perovskite like $(A_{n-1}B_nO_{3n+1})$ layers. Modification in these ceramics by doping to improve the properties of Aurivillius type of ceramics has been a matter of interest. These ceramics

show high value of Curie temperature and fatigue resistance, but suffer from high dielectric loss and low dielectric constant for which presence of free charges in the structure is believed to be the reason. A lot of research has been carried out to improve the properties of CBNO by doping different ions on the A-site of the perovskite structure.[17-20] It is reported that this substitution of some divalent (i.e., Ba^{2+}, Sr^{2+}) or trivalent (i.e., La^{3+}, Bi^{3+}) ions in the $(Bi_2O_2)^{2+}$ layers induces a transition from normal ferroelectric to a relaxor-like ferroelectric.[36-37] The Sr-substituted CBNO ceramics also exhibits a dielectric behavior. Therefore, in the present work a detailed investigation has been made to understand the effect of Sr substitution on the structure and dielectric properties of CBNO ceramic.

Experimental details

Stoichiometric samples of $Ca_{1-x}Sr_xBi_2Nb_2O_9$ (with x = 0.0, 0.5, 1.0) were prepared by conventional solid-state reaction method. High purity chemicals of $CaCO_3$, $SrCO_3$, Bi_2O_3 and Nb_2O_5 of AR grade were used as starting materials for the preparation of bulk samples. All the powders were weighed in a desired weight ratio and then grinded for two hours. The mixture was then divided into three equal parts and each part was then calcined at 800, 900, 1000°C, respectively for 5 hours in a programmable furnace with an increase in the temperature at the rate of 5°C /min. and then allowed to cool into the furnace. The cooled samples were then grinded and X-ray diffraction patterns were obtained using X-ray diffractometer (Miniflex-II, Rigaku). The powder was pressed at 15 MPa to form pellets of diameter ~ 13mm. Poly-vinyl alcohol (PVA) was used as a binder (3% by weight). The PVA was removed by further sintering at different temperatures.

The dielectric and impedance measurements were carried out by using an impedance/gain phase analyzer (Newtons4th Ltd.) in the frequency range from 1Hz to 10MHz at different temperatures by applying a small signal of 30mV in magnitude. The real (ε′) and imaginary (ε′′) parts of dielectric constant, loss tangent (tan δ) and conductivity were calculated using the following relations:

$$\varepsilon' = \frac{Z''}{2\pi f C_0 \left(Z'^2 + Z''^2\right)} \quad (1)$$

$$\varepsilon'' = \varepsilon' \tan\delta \quad (2)$$

$$\sigma = \varepsilon_0 \varepsilon' \omega \tan\delta \quad (3)$$

where C_0 is the capacitance of the sample in free space; Z′ and Z′′ are real and imaginary components of complex impedance; ε_0 is the free space permittivity and ω is the angular frequency.

3. Results and discussion

3.1. Structural studies

The X-ray powder diffraction patterns of $Ca_{1-x}Sr_xBi_2Nb_2O_9$ (x = 0.0, 0.5, 1.0) ceramics annealed at 1000°C are shown in Figure1.

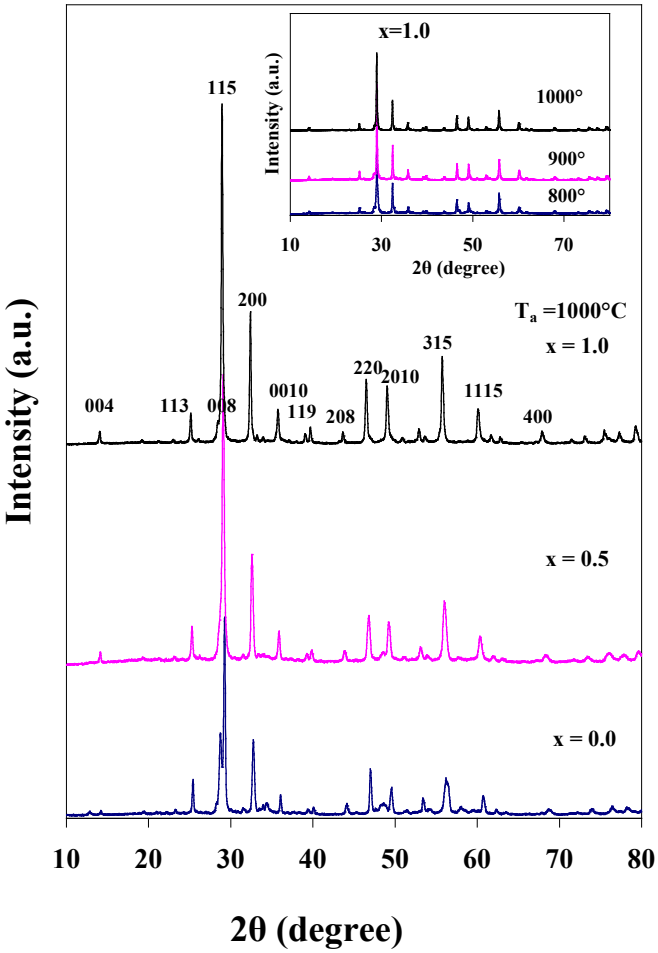

Figure 1 X-ray diffraction patterns of $Ca_{1-x}Sr_xBi_2Nb_2O_9$ (x = 0.0, 0.5, 1.0) ceramics at T_a= 1000°C, Inset: XRD patterns for` $SrBi_2Nb_2O_9$ (x = 1.0) ceramic at different annealing temperatures.

XRD results indicate that single phase layered perovskite were formed within the composition range studied in the present work without any detection of secondary phase. This reveals that the lower processing temperature is required to prepare the present samples. The position and intensity of intense peaks suggest the formation of perovskite structure in all the sintered samples. Lattice parameters have been calculated from the d-values obtained from the XRD data. It is observed that the peaks in the pattern for x = 0.0 ceramic belongs to orthorhombic structure with end centered symmetry and having space group $A2_1am$. For x = 0.5 and 1.0 ceramics the same orthorhombic structure with space group $A2_1am$ is observed. In the XRD pattern for x = 0.0 sample the strongest peak (115) at an angle of 29.230° match the main phase of orthorhombic structure (ICDD# 490608). Similarly the strongest peaks at 29.141° and 28.951° in the XRD pattern for x = 0.5 and x = 1.0 samples, respectively match the main phase of orthorhombic structure (ICDD# 00-060-0791 and ICDD# 490607). The lattice parameters for all the samples (along with the sample codes) for the strongest peak (115) are given in Table 1.

The average crystallite size (D) of prepared samples has been calculated using the following Debye-Scherrer's formula:

Table 1. Latticeparameters (a, b, c) of $Ca_{1-x}Sr_xBi_2Nb_2O_9$ ceramics for the strongest peak (115) at annealing temperature of 1000°C

x	Sample code	2θ	a (Å)	b (Å)	c (Å)
0.0	CBNO	29.230°	5.481	5.441	24.897
0.5	CSBNO	29.141°	5.444	5.468	25.105
1.0	SBNO	28.951°	5.523	5.513	25.120

Table 2. Lattice constant (L), average crystallite size (D), dielectric constant (ε′), loss tangent (tan δ) and ac conductivity (σ_{ac}) of $Ca_{1-x}Sr_xBi_2Nb_2O_9$ ceramics.

x	L (Å)	D (nm)			ε′(x10^5)	tan δ	σ_{ac} (Ωm)$^{-1}$
		T_a = 800°C	900°C	1000°C	at 1KHz, 300°C, T_a=1000°C		
0.0	15.86	37.5	40.3	39.0	0.06	23.5	0.009
0.5	15.91	22.0	33.0	30.7	0.10	11.4	0.020
1.0	16.01	36.6	41.3	38.0	0.08	7.80	0.005

$$D = \frac{k\lambda}{\beta \cos\theta} \quad (4)$$

where k = 0.9 (constant), λ is the X-ray wavelength, β is the full width at the half maximum of the most intense peak (115) and θ is the diffraction angle of the peak.[21]

The average crystallite size for different samples is given in the Table 2. The effect of annealing temperature on the formation of crystalline phase for SBNO(x = 1.0) ceramic is shown as insert of Figure 1. It is observed that the intensity of all the peaks increase with increase in the annealing temperature and this may be attributed to the increase in grain growth with the increase in annealing temperature.

Lattice constant (L) of all the samples has also been calculated from the XRD data and is found to increase almost linearly with increase in x (Table 2). The increase in lattice constant (L) may be attributed to the increase in grain growth with the increase in annealing temperature.

3.2. Dielectric studies

The dielectric properties of all the samples were studied at different temperatures and frequencies. Figure 2 shows the variation in dielectric constant (ε′) with frequency at different temperatures.

This indicates a strong dispersion of ε′ at low frequencies and a weak dispersion in the high frequency region, which suggests that the dispersion at higher frequencies is coupled with the space charge carriers. At low temperatures the dispersion curve in low frequency region show a broad hump which disappears as temperature increase. Also the peak of this hump slightly shifts to lower frequency region with the increase in temperature. This kind of behavior may be ascribed due to the relaxation process of space charge carriers. A similar kind of dispersion at low frequencies is also observed in the imaginary part of dielectric constant (i.e., ε′′). Such strong dispersion in both components of complex permittivity seems to be a common feature of ferroelectrics with good ionic conductivity.[22]

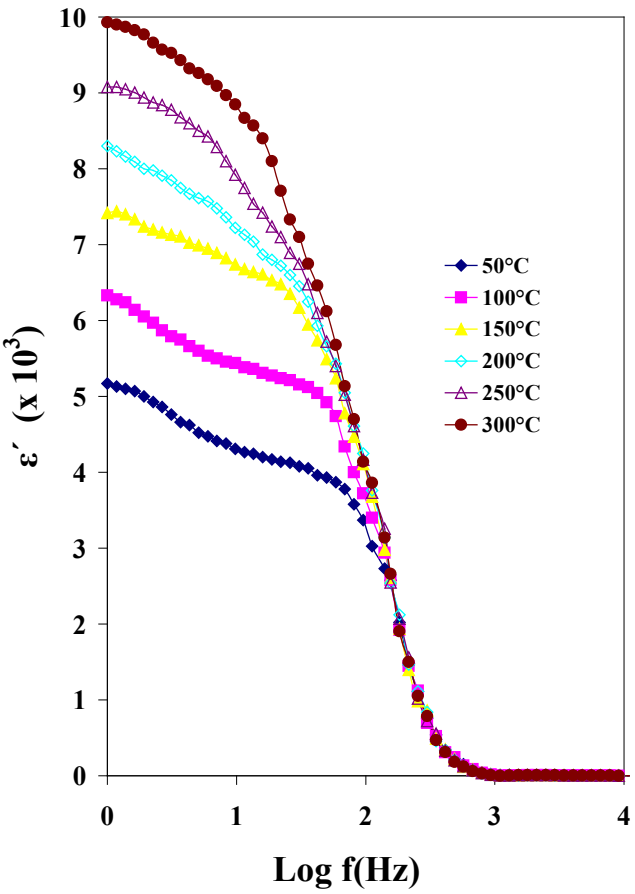

Figure 2 Frequency dependence of dielectric constant for $SrBi_2Nb_2O_9$ (*x* = 1.0) ceramic at various temperatures.

Figure 3(a) shows the variations of ε′ as a function of temperature at different frequencies. This figure indicates an

increasing trend of ε′ with temperature and it's values are high for low frequency. This is due to the coupling between charge carriers taking place in the polarization processes. It is believed that the ion-ion coupling is stronger in the low

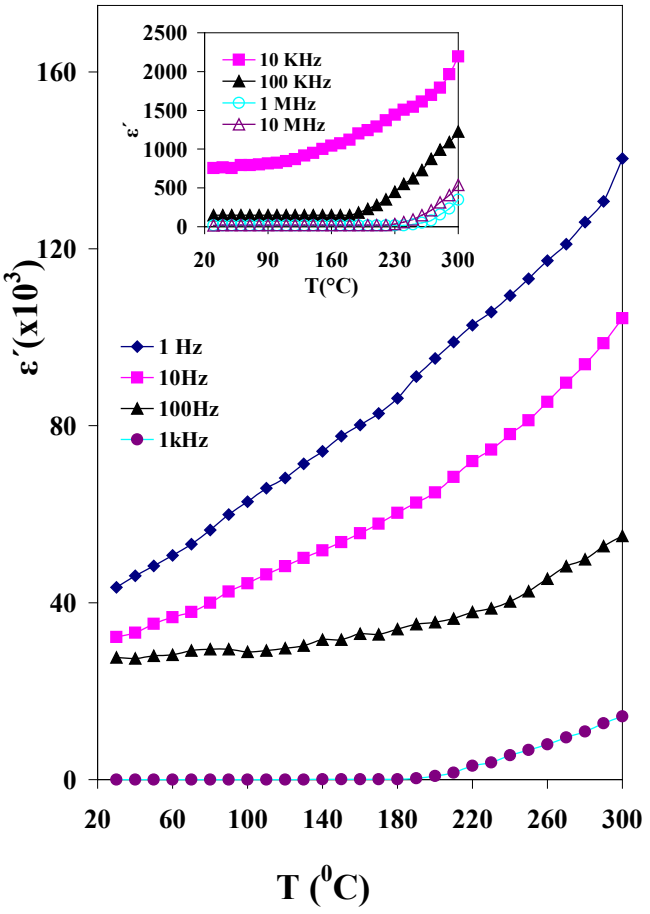

Figure3 (a) Temperature dependence of dielectric constant for $SrBi_2Nb_2O_9$ ceramic (x = 1.0, T_a = 1000°C) at various frequencies (1Hz to 1KHz); Inset; from 10 KHz to 10 MHz.

temperature region and as the temperature increases the number of space charge carriers increases. This behavior is also responsible for strong dispersion of dielectric constant (ε′) at low frequencies. Figure 3(b) shows that the value of ε′ increases more rapidly for CSBNO ceramic than for CBNO and SBNO above 200°C. This may be ascribed as due to the larger ionic radii of both Ca and Sr ions and at high temperature they form more conducting ions as compared with x = 0.0 and x = 1.0 samples. Recently, detailed structural studies for CBNO have shown that there is substantial cation place exchange between Ca^{2+} and Bi^{3+}.[23, 24] Therefore, we consider that for CSBNO, partial Sr^{2+} ions may occupy Bi sites in the Bi_2O_2 layers, and thus a small amount of Bi^{3+} would be incorporated into A sites in the perovskite- like layers. To maintain the electroneutrality, oxygen vacancies would be generated.

It was also reported that for $ABi_2Nb_2O_9$ (A = Ca, Sr, Ba) ceramics,[35] the degree of cation disorder between Bi^{3+} and A^{2+} increases with an increase in the A site cation size, i.e., Ca <

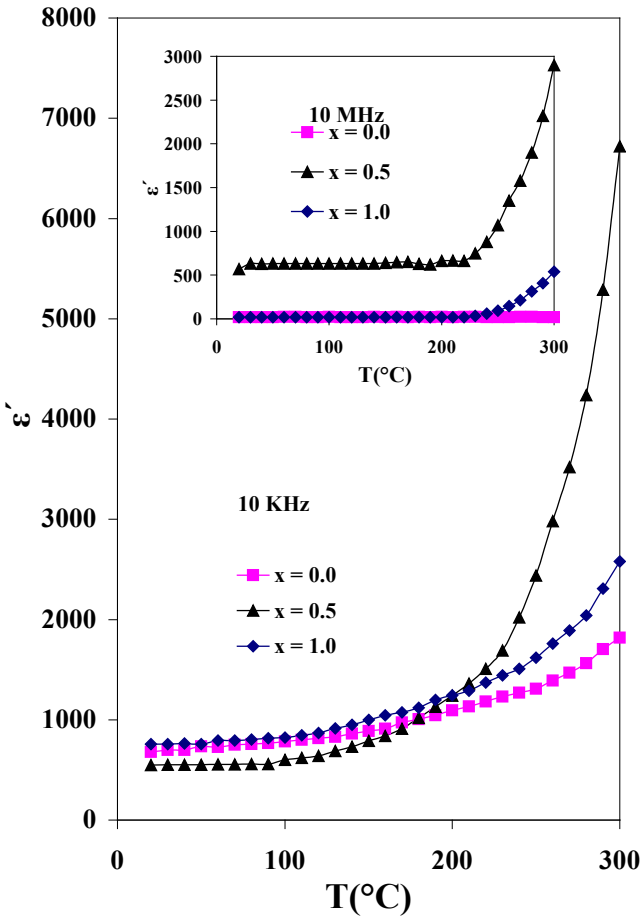

Figure 3(b) Temperature dependence of dielectric constant for $Ca_{1-x}Sr_xBi_2Nb_2O_9$ ceramics at 10 KHz; Inset: at 10 MHz

Sr < Ba. The bond energy, ionic radii and coordination number of different ions are given in Table 3 for comparison. However, the various synthesis conditions (temperature, time etc.) may result in structural disorder, which need to be further studied.[25] In the present case the magnitude of ε′ right from room temperature to 300°C is higher for SBNO ceramic as compared with CBNO sample at lower frequencies (Figure 3b). The excessive porosity associated with CBNO ceramics had led to the lower values of dielectric constant. The higher ε′ of SBNO samples indicates an increase in polarizability, arising out of the increased rattling space owing to the incorporation of much larger Sr ion in Ca sites apart from higher connectivity as these are very dense. Further Figure 4 shows dielectric loss (tan δ) as a function of temperature at different frequencies. It is clearly observed from this curve that the value of tangent loss is much lower for higher frequencies and remains almost constant at all the temperatures studied in the present work. Also the tangent loss increases with increase in temperature for frequencies lower than 10kHz. The values of ε′ and tan δ at 1kHz and 300°C are presented in Table 2 for all the samples. It is clear from the table that CSBNO sample has high ε′ and low tanδ than those for CBNO and SBNO samples thereby making it more suitable for electrical and electronic applications.

Table 3. Bond energy, ionic radii, and coordination number of various ions.

Ion	Bond Energy (KJ/mole)	Ionic Radius (Å)	Coordination Number	Reference
Ca^{2+}	403	1.36	12	25
Sr^{2+}	426	1.44	12	25
Bi^{3+}	336	0.96	5	34
Nb^{5+}	703	0.64	6	34

3.3. Impedance spectroscopic studies

Complex impedance analysis is a well known and powerful tool which has been effectively used for probing into the dielectric materials. This analysis enables one to resolve the contribution of various processes such as the electrode effects, bulk effects and interfaces, viz., the grain boundaries etc in the frequency domain. Figure 5 shows the frequency dependence

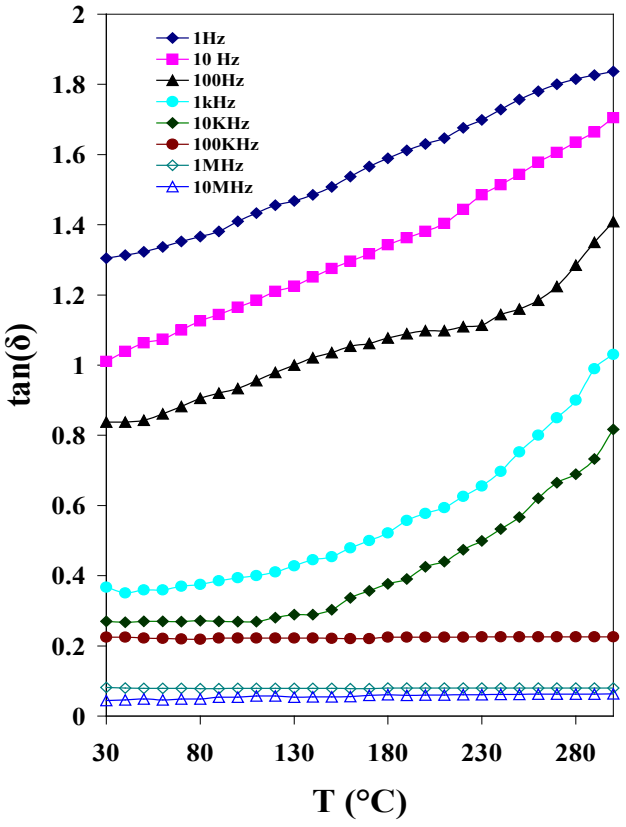

Figure 4 Temperature dependence of loss tangent (tanδ) for $Ca_{1-x}Sr_xBi_2Nb_2O_9$ ceramic (x = 1.0, T_a= 1000°C) at different frequencies.

of the imaginary part of impedance (Z′′) at different temperatures for SBNO ceramic (T_a = 1000°C). At low temperature (up to 200°C) there is a distinct sharp peak in the low frequency region which indicates a single relaxation process. The peak broadens with increase in temperature (>200°C) suggesting that relaxation occurs over several decades of frequency. The frequency (f_o) corresponding to maximum value of Z′′ (Z''_{peak}) shifts towards higher frequencies with increasing temperature. Also, it is clear from the figure that, irrespective of the temperatures at which the measurements are made, all the curves merge at higher frequencies. At higher frequencies, the contribution from the grain predominates owing to the absence of the space charge effects. The relaxation time (τ) associated with each peak was obtained by using the equation $\tau = 1/2\pi f_0$. However, the broadening of peak above 200°C suggests the distribution of relaxation times and the contribution comes from grain (at high frequency) and grain boundaries (at low frequency).

A similar kind of behavior is observed in CSBNO ceramics. But in CBNO sample there is only one distinct peak from room temperature to 300°C temperature range. This indicates that the contribution from the grain boundary is absent in this sample. This single distinct peak, corresponding to the bulk sample, shifts to higher frequencies as the temperature is increased. It is believed that the grain boundary contribution is minimized due to the closely packed uniform microstructure of the CBNO ceramics.

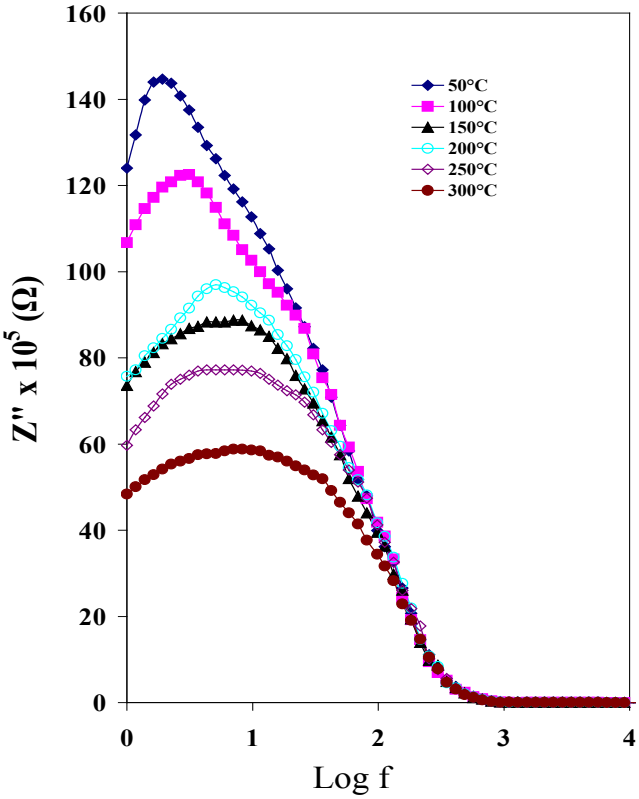

Figure5 Frequency dependence of imaginary part of impedance (Z′′) for $Ca_{1-x}Sr_xBi_2Nb_2O_9$ ceramic (x = 1.0, T_a=1000°C) at various temperatures.

Table 4. Grain resistance (R_g), bulk capacitance (C_g) and relaxation frequency (f_o), at different temperatures for $CaBi_2Nb_2O_9$ (x = 0.0)ceramic sintered at 1000°C.

Temperature (°C)	R_g (MΩ)	C_g (μ F)	f_o (Hz)
50	0.195	0.83	351
100	0.298	0.53	298
200	0.392	0.41	163
300	0.576	0.27	156

3.4 Cole – Cole plots

In the complex impedance plot (Cole-Cole; Z′ vs. –Z′′ plotted in a linear scale), depending on the relative values of their relaxation times, generally data give rise to three semicircular arcs. The arc at high frequency end refers to the bulk electrical conduction, the intermediate arc corresponds to conduction by grain boundaries and the arc at low frequency end arises from electrode processes. Each of these semicircles could be represented by a single RC combination. A depressed semicircle whose centre lies below the real axis suggests the departure from the ideal Debye behavior.[26-28] The semicircle passes through a maximum at a frequency f_o (relaxation frequency) and satisfies the condition

$$\omega\tau = 1 \qquad (5)$$

Figure 6 shows the Cole-Cole plots for CBNO sample at various temperatures in the frequency range from 1Hz – 10 MHz. These plots show only one semi circle with its centre lying below the real axis for the whole range of temperature covered in the present study. This clearly indicates a single conduction mechanism originating from grain (bulk) is prevailing in the sample. The absence of second semicircle suggests that there is no contribution from grain boundary resistance in the samples. The complex impedance in this model is expressed by the equation

$$Z^*(\omega) = Z^*_{bulk} + Z^*_{gb} \qquad (6)$$

Where

$$Z^*_{bulk} = \frac{R}{1 + CR j\omega + A_o R (j\omega)^n} \qquad (7)$$

And

$$Z^*_{gb} = \frac{R_{gb}}{1 + B_o R_{gb} (j\omega)^m} \qquad (8)$$

A_o, B_o, n and m are the temperature dependent parameters. These parameters can be calculated by the curve fitting method using the complex nonlinear least-squares fitting[17] of both real and imaginary parts of the complex impedance.

Also it is observed from Figure 6 that with increase in temperature the semicircles shift towards higher Z′ values indicating an increase in the impedance of both the grain and grain boundary. Similar kind of behavior is observed in other samples. It was also observed that the value of bulk resistance increases with increase in value of 'x'. Also the values of the bulk resistance for the CSBNO ceramic are found to be higher by one order of magnitude, than that for CBNO ceramic. The impedance diagram in the temperature range 50°C – 300°C could be modelled by an equivalent electrical circuit comprised of set of resistance and capacitance in parallel. The low frequency intercept made by the semicircle on the real impedance axis could be used to determine the bulk resistance of the sample while the capacitive values are obtained from the frequency corresponding to the highest point in each semicircle. The values of grain resistance (R_g), bulk capacitance (C_g), and relaxation frequency (f_o) through which the semicircle pass are listed in Table 4. The above analysis of electric and dielectric properties of the prepared ceramics allows us to find the equivalent electrical circuits by using the calculated values of resistance and capacitance in different

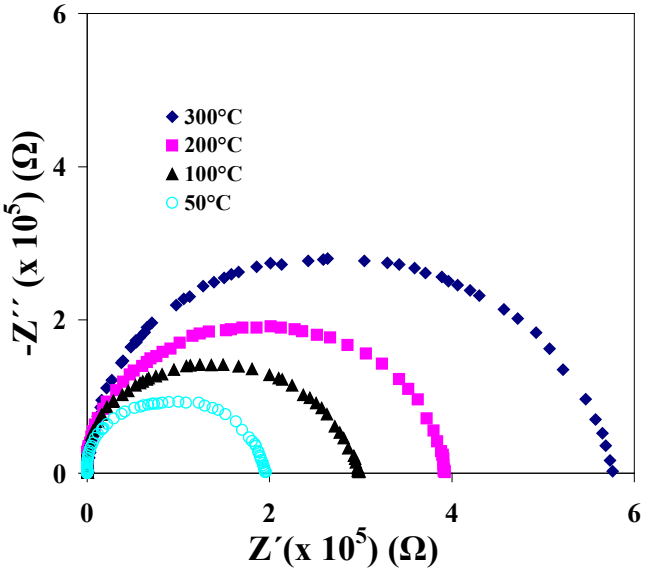

Figure 6 Complex impedance plots at different temperatures for$CaBi_2Nb_2O_9$ ceramic (x = 0.0, T_a =1000°C)

boundary regions. However the source of distribution of relaxation times is the existence of inhomogeneity in the electrical conductivity and can be described in the circuits by the CPE (constant phase element). It might be caused by different concentrations of Sr^{2+} cations in Bi_2O_2 slabs and consequently the concentration of oxygen vacancies may vary in different parts of the sample.

3.5. Complex modulus plots

Complex modulus formalism is very important and convenient tool to determine, analyze and interpret the

dynamical aspects of electrical transport phenomena, i.e., parameters such as carrier/ion hopping rate, conductivity time relaxation etc.[29-30] since each dielectric function has its own distinct relaxation time which indicates that a particular process can be represented by not one but several relaxation times, depending on the dielectric function chosen. The real and imaginary part of the modulus functions are expressed by the following

$$M^* = j\omega C_o Z^* \qquad (9)$$

$$M' = \frac{\varepsilon'}{\varepsilon'^2 + \varepsilon''^2} \qquad (10)$$

$$M'' = \frac{\varepsilon''}{\varepsilon'^2 + \varepsilon''^2} \qquad (11)$$

In the above equation ω is the angular frequency (= $2\pi f$), C_o is the vacuum capacitance of the measuring cell and electrodes with an air gap of the dimensions of the sample thickness. So, we have also adopted the modulus formalism to study the relaxation in CSBNO ceramics.

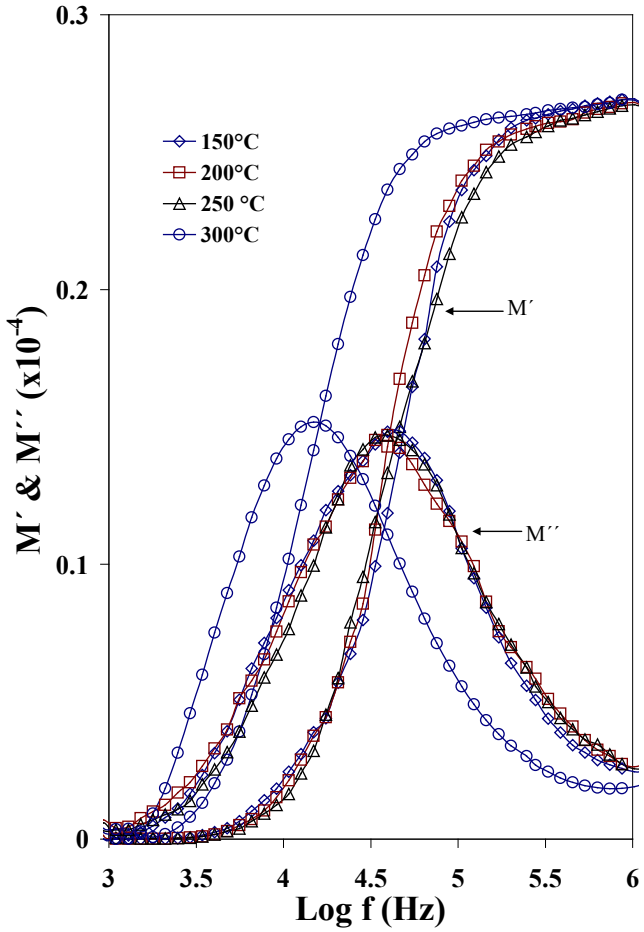

Figure7 Frequency dependence of real (M′) and imaginary (M′′) parts of electric modulus at different temperatures for $Ca_{0.5}$ $Sr_{0.5}Bi_2Nb_2O_9$ (x = 0.5, T_a =1000°C).

Figure 7 shows the frequency dependence of complex modulus (M′ and M′′) at different temperatures. The peak in M′′ vs. log (f) curve indicates the single relaxation process in the high frequency region, and also the peak shifts towards lower frequency side with increase in temperature. This indicates the increase in relaxation time with decrease in frequency. [31-33] One can determine the most probable relaxation time from the position of the peak in the M′′ vs. log (f) curve. The most probable relaxation time obeys the Arrhenius law given by:

$$\tau_m = \tau_o \exp\left[\frac{-E_a}{k_B T}\right] \qquad (12)$$

where τ_o is the pre-exponential factor, k_B is the Boltzmann constant and E_a is the activation energy for the corresponding process. Since the change in dielectric constant of the grain boundary phase is small (almost constant) with temperature, the change in the value of M′′ indicates the grain contribution. The frequency plots of the imaginary parts of the impedance and modulus indicates departure from ideal Debye behavior. The peaks of Z′′ and M′′ are not in coincidence with each other which suggest a deviation from the Debye behavior. Both the Z′′ vs. log f and M′′ vs. log f plots are asymmetric for all the samples studied. A shift in

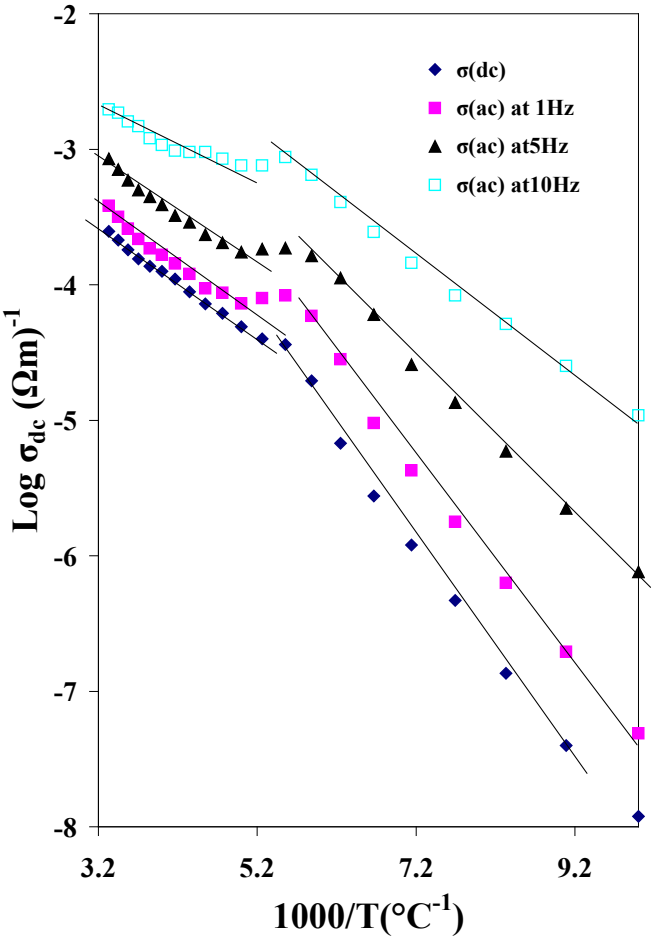

Figure 8 The inverse temperature dependence of conductivity at various frequencies for $SrBi_2Nb_2O_9$ (x = 1.0) ceramic.

maximum frequency and a corresponding change in the maximum value of M´´ in all the samples would suggest a variation in the capacitance. Also, M´ shows a dispersion behavior tending towards M_∞ where, M_∞ is the asymptotic value of M´ at higher frequencies.

3.6.DC conductivity

The conductivity of grains (σ_{DC}) of all the samples can be calculated by the relation

$$\sigma_{DC} = \frac{d}{sR} \qquad (13)$$

where 'd' is the thickness and 's' is the surface area of the sample. The results obtained were in good agreement with the Arrhenius formula, which indicates the thermal activation of the process (Figure 8). The presence of two regions with different activation energies (E_a) was observed. In lower temperature range $E_{a(lt)}$= 0.084 eV whereas in higher temperature range $E_{a(ht)}$ = 0.21 eV. The temperature at which the change in E_a occurs is equal to about 181.8°C. This temperature has no correlation with the ferroelectric phase transition temperature in the material. The activation energy of 1 eV value is connected with the oxygen vacancy motion. The temperature at which the grain resistance dominates over the grain boundary resistance, there is a change in the slope of a.c conductivity with frequency.[18] The frequency at which the slope change is observed corresponds to polaron hopping of charged species. The polaron hopping frequency is observed to shift to lower frequencies with increasing temperature indicating increasing conductivity with temperature.

With increasing temperature the charged species that are accumulated at the grain boundaries have sufficient energy to jump over the barrier, thereby increasing the conductivity. Thus the grain boundary resistance decreases beyond this frequency and temperature.

AC conductivity

For a better understanding of the influence of the electrical conductivity on the ferroelectric properties, the obtained data of CSBNO sample were plotted as a function of frequency to represent the variation in the real part of ac conductivity (σ_{ac}) as shown in Figure 9. It can be seen that the plateau of conductivity, i.e., frequency independent values of conductivity, corresponding to the dc conductivity, was observed in the low frequency region at high temperatures. In the higher frequency region, the strong dispersion of electric conductivity was observed and the changes of $\sigma(f)$ in this region can be described as proportional to f^n, where 'n' is the parameter depending on the temperature.[34] The character of these changes does not depend on temperature. Although with the increase in temperature it was noted that the range of frequency where dispersion occurs moved to higher frequencies.

A similar tendency was observed for CBNO and SNBO samples. Earlier this kind of behavior was observed in $SrBi_2Ta_2O_9$ ceramic.[20]

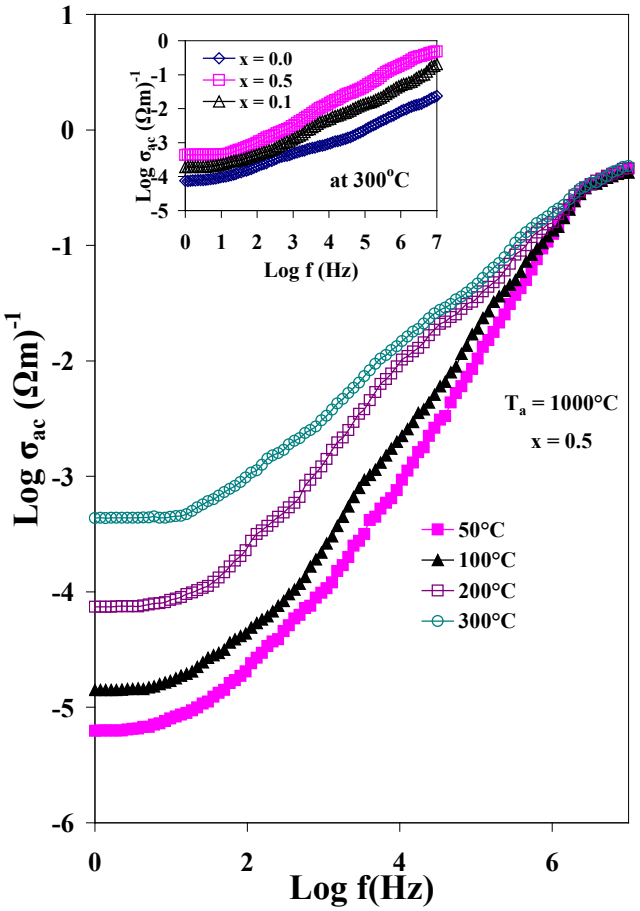

Figure 9 Frequency dependence of ac conductivity σ_{ac} at different temperatures for $Ca_{1-x}Sr_xBi_2Nb_2O_9$ ceramic (x = 0.5); Inset: composition dependence of ac conductivity of $Ca_{1-x}Sr_xBi_2Nb_2O_9$ ceramic at 300°C.

Conclusions

$Ca_{1-x}Sr_xBi_2Nb_2O_9$ (x = 0.0, 0.5, 1.0) ceramics were successfully synthesized by conventional solid-state reaction method. X-ray diffraction shows that the samples belong to orthorhombic structure having space group $A2_1am$ with end centered symmetry. The dielectric and impedance behavior of these ceramics were investigated over a wide range of frequency and temperatures. The maximum value of dielectric constant ε´ and corresponding low dielectric loss (tanδ) was observed in the samples with x = 0.5. Impedance spectroscopic studies revealed that the material exhibited relaxation effects and the frequency dependent plots of imaginary components of impedance and modulus suggested the relaxation to be of non-Debye type. The observed dielectric relaxation was ascribed to the thermally activated motion of ionized oxygen vacancies. The bulk resistance calculated from Cole-Cole plot gave the values of grain resistance which indicates that the conductivity mechanism is dominated by grain interior conduction. Grain resistance is found to increases with increase in temperature and with value of 'x'. From the ac conductivity plots it was observed that the electrical conductivity obeyed the universal power law dependence.

References and notes

1. B. Aurivillius, 'Mixed Bismuth Oxides with layer lattices :1, Structure type of $CaBi_2B_2O_9$',*Ark. Kemi*, **1952**, 4, 39.
2. A. Ando, T. Sawada, H. Ogawa, M. Kimura, Y. Sakabe, 'Fine tolerance resonator applications of Bismuth-Layer-Structured ferroelectric ceamics', *Jpn. J. Appl. Phys*., **2002**, 41, 7057.
3. A. Ando, M. Kimura, T. Minamikawa, Y. Sakabe, ' Layered piezoelectric ceramics for fine-tolerance resonator applications', *Int. J. Appl. Ceramic Technol*. **2005**, 2, 33.
4. P. Milan, A. Castro, J. B. Torrance, 'The first doping of Pb_{2+} into the bismuth oxide layers of the C oxides', *Mater. Res. Bull*. **1993**, 28, 117.
5. A. Castro, P. Milan, R. Enjalbert, 'Structural evolution of the Aurivillius framework in the solid solutions of Bi_2WO_6-Sb_2WO_6', *Mater. Res. Bull*. **1995**, 30, 871.
6. P. Milan, A. Ramirez, A. Castro, ' Substitution of smaller Sb^{3+} and Sn^{2+} cations for Bi^{3+} in Aurivillius like phases', *J. Mater. Sci. Lett*. **1995**, 14, 1657.
7. S. B. Desu, D.P. Vijay, 'Novel fatigue-free layered structure ferroelectric thin film', *Mater. Sci. Eng. B* **1995**, 32, 75.
8. C. A. Paz de Araujo, J. D. Cuchlaro, L. D. McMillan, M. C. Scott, J. F. Scott, 'Fatigue-free ferroelectric capacitors with platinum electrodes', *Nature*. **1995**, 374, 627.
9. J. F. Scott, F. M. Rose, C. A. Paz de Araujo, M. C. Scott, M. Huffman, ' Structure and device characteristics of $SrBi_2Ta_2O_9$-based nonvolatile random-access memories', *MRS Bull*. **1996**, 21, 33.
10. T. K. Li, Y. Zhu, S. B. Desu, C. Peng, M. Nagata, 'Metalorganic chemical vapour deposition of ferroelectric $SrBi_2Ta_2O_9$ thin film', *Appl. Phy. Lett*. **1996**, 86, 29.
11. E. C. Subba Rao, 'A family of ferroelectric bismuth compounds', J. *Phys. Chem. Solids.* **1962**, 23, 665.
12. T. Takenaka, K Sakata, ' Grain orientation and electrical properties of hot-forgrd $Bi_4Ti_3O_{12}$ ceramics', *Jap. J. Apply. Phys*. **1980**, 19, 31.
13. K. Katori, N. Nagel, K. Watanabe, M. Tanaka, H. Yamoto, H. Yagi, *9th Int. Symp. On Integrated Ferroelectrics (Santa Fe, NM),* **1997.**
14. M. Nagata, D. P. Vajay, X. Zhang, S. B. Desu, 'Formation and properties of $SrBi_2Ta_2O_9$ thin film', *Phys. Status Solidi*, **1996**, 157, 75.
15. C. H. Lu, C. Y. Wen, 'New non-fatigue ferroelectric thin film of barium bismuth tantalate', *Mater. Lett*. **1999**, 38, 278.
16. T. Chen, T. K. Li, X . Zhang, S. B. Desu, 'The effect of excess bismuth on the ferroelectric properties of $SrBi_2Ta_2O_9$ thin film', *J. Mater. Res*. **1997**, 12, 1569.
17. J. H. Bi, L. Wu, J. Li, Z. H. Li, X. X. Wang, 'Simple solvothermal routes to synthesize nanocrystalline Bi_2MoO_6 photocatalysts with different morphologies, *Acta Mater*. **2007**, 55, 4699.
18. S. P. S. Badwal, *"Proceedings of the International Seminar on Solid State Ionic Devices" (World Scientific Publishing, Singapore,* **1988**) p. 165.
19. S. M. Blake, M. J. Falconer, M. McCreedy, P. Lightfoot, 'Cation disorder in ferroelectric Aurivillius phase of the type $Bi_2ANb_2O_9$(A = BA, Sr, Ca)', *J. Mater. Chem*. **1997**, 7, 1609.
20. . C. Palanduz, D. M. Smyth, 'Defect chemistry and charge transportation in $SrBi_2Nb_2O_9$ ceramics', *J. Electroceram.* **2003**, 11, 191.
21. E. Barsoukov, J.R. Macdonald, *Impedance Spectroscopy Theory, Experiment and Applications, Second ed., Wiley-Interscience Press, New York,* **2005.**
22. D. C. Sinclair, A.R. West, 'Impedance and modulus spectroscopy of semiconducting $BaTiO_3$ showing positive temperature coefficient of resistance', *J. Appl. Phys*. **1989**, 66, 3850.
23. N. Shivasankara, A. Narayanswami, N. Ponpandian, 'Grain size effect on the dielectric behavior of nanostructured $Ni_{0.5}Zn_{0.5}Fe_2O_4$', *J. Appl. Phys*. **2007**, 101, 084116.
24. B. A. Boukamp, 'A linear Kroning-Kramers transform test for immittance data validation', *J. Electrochem. Soc*. **1995**, 142, 1885.
25. D. Dhak, P. Dhak, T. Ghorai, S. K. Biswas, P. Pramanic, 'Preparation of nano-sized $ABi_2Nb_2O_9$ (A = Ca, Sr, Ba) ferroelectric ceramics by soluble Nb tartarate precursor and their dielectric characterization after sintering', *J. Mater Sci*. **2008**, 19, 448.
26. K. Sriniwas, P. Sarah and S. V. Suryanarayna, 'Impedance spectroscopy study of polycrystalline $Bi_6Fe_2Ti_3O_{18}$', *Bull. Mater. Sci*. **2003**, 26, 247.
27. K. S. Rao, D. M. Prasad, P. M. Krishna, B. H. Bindu, K. Suneetha, 'Frequency and temperature dependence of electrical properties of barium and gadolinium substituted $SrBi_2Nb_2O_9$ ceramics', *J. Mater. Sci*., **2007**, 42, 7363.
28. A. R. James, S. Balaji, S. B. Krupanidhi, 'Impedance-fatigue correlated studies on $SrBi_2Ta_2O_9$ ', *Mater. Sci. Eng. B*. **1999**, 64, 149.
29. H. Yin, A.Zhou, N. Chang, X.Xu, 'Characterization and photocatalytic activity of Bi_3TiNbO_9 nanocrystallines synthesized by sol-gel process', *Mater. Res. Bull*. **2009**, 44, 377.
30. J. H. Bi, L. Wu, Z.Li, X. X.Wang, X. Z. Fu, 'A citrate complex process to prepare nanocrystalline PbBi2Nb_2O_9 at a low temperature', *Mater. Lett*. **2008**, 62, 155.
31. C. X. Xu, X. Wei, Z. H. Ren, Y. Wang, G. Xu, G. Shen, 'Olvothermal preparation of Bi_2Wo_6 nanocrystals with improved visible light photocatalytic activity', *Mater Lett*. **2009**, 63, 2194.
32. T. Takenaka, K Sakata, 'Composition and electrical properties of complex bismuth-layer-structured ferroelectric ceramics', *Jap. J. Appl. Phys*. **1985**, 24, 117.
33. T. Takenaka, K Sakata, 'Grain orientation effects on electrical properties of bismuth layer-structured ferroelectric $Pb_{(1-x)}(NaCe)_{x/2}Bi_4Ti_4O_{15}$ solid solition', *J. Appl. Phys*. **1984**, 55, 1092.
34. A. J. Moulson, J. M. Herbert, *Electroceramics* (*Chapman and Hall, London,* **1990**).
35. S. Khasa, M. Dahiya, A. Agarwal. Structural Investigations of Lithium Vanadoxide Bismo-Borate Glasses. *J. Integr. Sci. Technol.*, **2013**, 1(1), 44-47.
36. V. Kumar, A.K. Bedyal, H.C. Swart, O.M. Ntwaeaborwa. Spectral and surface investigations on SrZnO2:Tb3+ nanophosphors. *J. Integr. Sci. Technol.*, **2013**, 1(1), 19-22.
37. R. Prakash. Growth and study of PrCoO3 thin films nanostructures deposited on various substrates. *J. Integr. Sci. Technol*., **2013**, 1(1), 1-4.